Springer Series
in Biophysics 13

N. G. Walter · S. A. Woodson · R. T. Batey (Eds.)

Non-Protein Coding RNAs

This book assembles chapters from experts in the Biophysics of RNA to provide a broadly accessible snapshot of the current status of this rapidly expanding field. The 2006 Nobel Prize in Physiology or Medicine was awarded to the discoverers of RNA interference, highlighting just one example of a large number of non-protein coding RNAs. Because non-protein coding RNAs outnumber protein coding genes in mammals and other higher eukaryotes, it is now thought that the complexity of organisms is correlated with the fraction of their genome that encodes non-protein coding RNAs. Essential biological processes as diverse as cell differentiation, suppression of infecting viruses and parasitic transposons, higher-level organization of eukaryotic chromosomes, and gene expression itself are found to largely be directed by non-protein coding RNAs. The biophysical study of these RNAs employs X-ray crystallography, NMR, ensemble and single molecule fluorescence spectroscopy, optical tweezers, cryo-electron microscopy, and other quantitative tools. This emerging field has begun to unravel the molecular underpinnings of how RNAs fulfill their multitude of roles in sustaining cellular life. The physical and chemical understanding of RNA biology that results from biophysical studies is critical to our ability to harness RNAs for use in biotechnology and human therapy, a prospect that has recently spawned a multi-billion dollar industry.

ISSN 0932-2353

ISBN 978-3-540-70833-9

springer.com

Walter · Woodson
Batey (Eds.)

Non-Protein Coding RNAs

Springer Series
in Biophysics 13

Nils G. Walter
Sarah A. Woodson
Robert T. Batey (Eds.)

Non-Protein Coding RNAs

Springer

Chapter 5
The Small Ribozymes: Common and Diverse Features Observed Through the FRET Lens

Nils G. Walter(✉) and Shiamalee Perumal

Abstract The hammerhead, hairpin, HDV, VS and *glmS* ribozymes are the five known, naturally occurring catalytic RNAs classified as the "small ribozymes." They share common reaction chemistry in cleaving their own backbone by phosphodiester transfer, but are diverse in their secondary and tertiary structures, indicating that Nature has found at least five independent solutions to a common chemical task. Fluorescence resonance energy transfer (FRET) has been extensively used to detect conformational changes in these ribozymes and dissect their reaction pathways. Common and diverse features are beginning to emerge that, by extension, highlight general biophysical properties of non-protein coding RNAs.

5.1 Introduction

Since the discovery in the early 1980s that certain biological catalysts involved in the processing of genetic information are composed of RNA (Kruger et al. 1982; Guerrier-Takada et al. 1983), a number of such natural ribozymes have been discovered, and research in the field has focused on elucidating their enzymatic mechanisms and secondary and tertiary structures. In recent years, the spotlight has been on emerging high-resolution crystal structures that illustrate the precise manner in which ribozymes orient and align reactive groups. The main challenge now lies in linking these static snapshots to the dynamical features of RNA structure to answer the outstanding question of how chemical catalysis arises. This chapter summarizes how the current application of fluorescence resonance energy transfer (FRET) has helped dissect the reaction mechanisms of the small ribozymes. Common and distinct features are beginning to emerge under the magnifying lens of FRET.

N.G. Walter
Department of Chemistry, University of Michigan, Ann Arbor, 93. N University, MI 48109–1055, USA
e-mail: nwalter@umich.edu

N.G. Walter et al. (eds.) *Non-Protoin Coding RNAs*

doi: 10.1007/978-3-540-70840-7_5,

5.2 The Class of Small Ribozymes

5.2.1 Common Mechanism and Catalytic Strategies

Biological evolution has produced and preserved five known, structurally distinct ribozymes that promote non-hydrolytic phosphodiester backbone cleavage in RNA, the hammerhead, hairpin, hepatitis delta virus (HDV), Varkud satellite (VS), and *glmS* ribozymes. Given their relatively small size (<200 nt) and common reaction mechanism, these self-cleaving RNAs are grouped as the class of "small ribozymes" (Doudna and Lorsch 2005; Fedor and Williamson 2005; Bevilacqua and Yajima 2006; Scott 2007). Unlike their larger counterparts, such as group I and II intron ribozymes or RNase P, the small ribozymes do not require an external nucleophile but site-specifically activate one of their own 2′-OH moieties by de-protonation to attack the adjacent 3′, 5′-phosphodiester and substitute the 5′-oxygen in an S_N2-type phosphodiester transfer. As a result, the 5′- and 3′-reaction products carry 2′, 3′-cyclic phosphate and 5′-OH termini, respectively (Fig. 5.1).

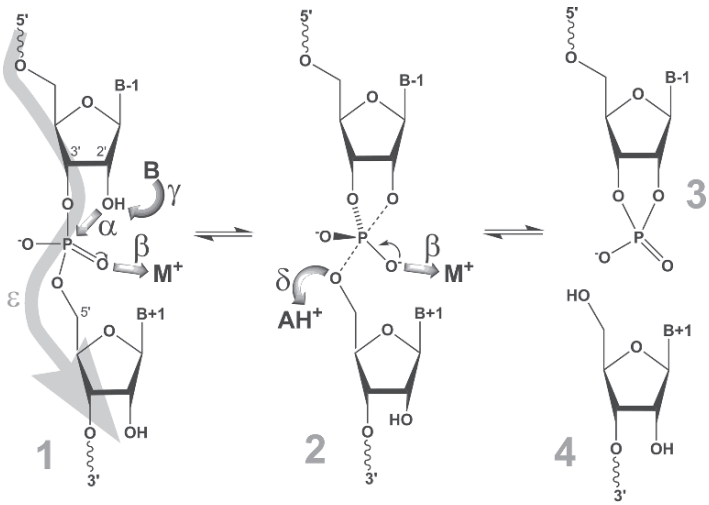

Fig. 5.1 Mechanism of RNA cleavage by the small ribozymes. The backbone (**1**) passes through a penta coordinate transition state (**2**) that degrades into the 5′- and 3′-cleavage products carrying 2′, 3′-cyclic phosphate (**3**) and 5′-hydroxyl termini (**4**), respectively. Five catalytic strategies that can promote the reaction mechanism are highlighted by broad shaded arrows and Greek letters: α, in-line nucleophilic attack of the 2′-oxygen on the scissile phosphate at an idealized 2′O-P-5′O angle of 180°; β, neutralization of the negative charge on a non-bridging phosphate oxygen; γ, deprotonation of the 2′-hydroxyl group by a base B; δ, protonation of the developing negative charge on the 5′-oxygen leaving group by an acid AH^+; and ε, ground state structure destabilization (substrate straining)

Although many protein-based ribonucleases catalyze the same reaction, the small ribozymes afford superior site-specificity by using base pairing and other interactions, to align the cleavage site for in-line nucleophilic attack. Arguably, evolution chose these RNA-based catalysts not for their rate acceleration and capacity to process, which is higher for the protein enzymes, but for their compact usage of genetic information to accomplish unique sequence specificity. This sequence specificity is all the more surprising since the mechanism catalyzed is the same as that of the non-enzymatic degradation of RNA (Zhou and Taira 1998), which implies that a ribozyme has to avoid non-specific backbone cleavage while promoting the site-specific path.

The small ribozymes, though very different in chemical makeup, are turning out to use the same repertoire of catalytic strategies as their protein counterparts (Emilsson et al. 2003; Doudna and Lorsch 2005; Fedor and Williamson 2005; Bevilacqua and Yajima 2006; Scott 2007; Walter 2007), including (Fig. 5.1): positioning of the reacting functional groups in an optimal in-line attack configuration (α); electrostatic catalysis to stabilize the enhanced negative charge on the phosphate oxygens in the transition state (β); general base catalysis by removing the proton from the attacking 2′-OH nucleophile (γ); general acid catalysis by donating a proton to the 5′-oxygen leaving group (δ); and destabilization of the ground state structure (ε).

In protein-based enzymes, the chemical versatility of the amino-acid side chains contributes polar, charged or uncharged polar side chains as obvious participants in general acid–base and electrostatic catalysis. Initially, it was therefore less clear how ribozymes with their more limited chemical makeup may affect general acid–base catalysis at neutral pH, especially since ionization of the nucleobases and riboses in isolation only occurs at considerably acidic or basic pH. Consequently, the first proposals suspected external cofactors such as liganded, partially hydrated Mg^{2+}-ions as effectors of ribozyme chemistry (Pyle 1993); but the field has now embraced the idea of chemistry catalyzed by pK_a-shifted nucleobases (Doudna and Lorsch 2005; Fedor and Williamson 2005; Bevilacqua and Yajima 2006) and even considers mechanisms involving proton relays through structural water molecules (Walter 2007). Intriguingly, the field has come full circle through discovery of the *glmS* ribozyme, since this ribozyme indeed requires an external, small-molecule co-factor as an essential reaction participant (McCarthy et al. 2005; Hampel and Tinsley 2006; Klein and Ferre-D'Amare 2006; Tinsley et al. 2007).

The three questions to be specifically addressed in this review are: (i) How can FRET dissect the folding and reaction pathways responsible for positioning the participants of small ribozyme catalysis? (ii) How do small ribozymes direct catalytic power towards one specific bond without sacrificing their overall backbone integrity? (iii) Which common and diverse features emerge from a comparison of the five known, naturally occurring small ribozymes? We will address these questions by first summarizing what insights FRET has helped reveal for each small ribozyme.

5.3 The Hammerhead Ribozyme

The hammerhead ribozyme was first discovered in viroids and satellite RNAs of plant viruses, where it is thought to be essential for RNA self-cleavage and -ligation during double-rolling circle replication of the parasitic pathogen (Prody et al. 1986; Forster and Symons 1987; Flores et al. 2004). It was subsequently also identified in the genomes of the newt (*Notophthalamus viridescens*), schistosome trematodes, cave crickets (*Dolichopoda* species), and even mammals (Martick et al. 2008b) and emerges as the smallest and most common self-cleaving RNA motif from *in vitro* evolution experiments, suggesting that nature may have created it multiple times by convergent evolution (Salehi-Ashtiani and Szostak 2001).

The hammerhead motif consists of a catalytic core of 11 conserved nucleotides flanked by three helical stems that are arranged in a "Y-shape" by a sharp uridine (U-)turn in the backbone that juxtaposes Stems I and II (Ruffner et al. 1990; Wedekind and McKay 1998) (Fig. 5.2a). The ribozyme is catalytically active in the presence of either millimolar divalent or molar monovalent cations with similar sequence requirements, suggesting that divalents are not obligatory participants in phosphodiester transfer (Murray et al. 1998; Curtis and Bartel 2001; O'Rear et al. 2001). Most of the functional groups in the catalytic core are essential for catalytic activity (McKay 1996), making it initially difficult to distinguish moieties important for folding from those directly involved in catalysis. In addition, a controversy ensued between early crystal structures and biochemical evidence that suggested significant conformational changes from these structures were necessary to reach the catalytically active state (Blount and Uhlenbeck 2005).

Only in 2003 did it become clear that all naturally occurring hammerhead ribozymes have non-conserved (and therefore initially overlooked) loop–loop interactions between Stems I and II that further stabilize the Y-shape (Fig. 5.2b) and significantly enhance catalysis, especially at near-physiologic concentrations of Mg^{2+} (0.5–1 mM free Mg^{2+}) (De la Pena et al. 2003; Khvorova et al. 2003; Penedo et al. 2004).The controversy was lifted by new crystal structures including such loop–loop interactions by showing how these distal tertiary contacts rearrange the catalytic core, in a way much more consistent with the biochemical data, where the scissile phosphate is poised for general acid–base catalysis by functional groups of guanosines G8 and G12 (Martick and Scott 2006; Nelson and Uhlenbeck 2006) and potentially a structural water molecule (Martick et al. 2008a) (please note that these structures are the focus of the preceding chapter by Scott). The current, unifying model suggests that both the "minimal" and "extended" hammerhead ribozymes dynamically adopt both inactive and active conformations similar to the two types of crystal structures, albeit with different bias, leading to the observed difference in catalytic activity (Martick and Scott 2006; Nelson and Uhlenbeck 2008b; Nelson and Uhlenbeck 2008a).

The hammerhead ribozyme thus emerges as a small, yet very dynamic RNA motif, which has largely eluded high-resolution solution-phase structure determination for example by, NMR spectroscopy (Simorre et al. 1997; Simorre et al. 1998; Bondensgaard et al. 2002; Furtig et al. 2008). Fluorescence spectroscopy is

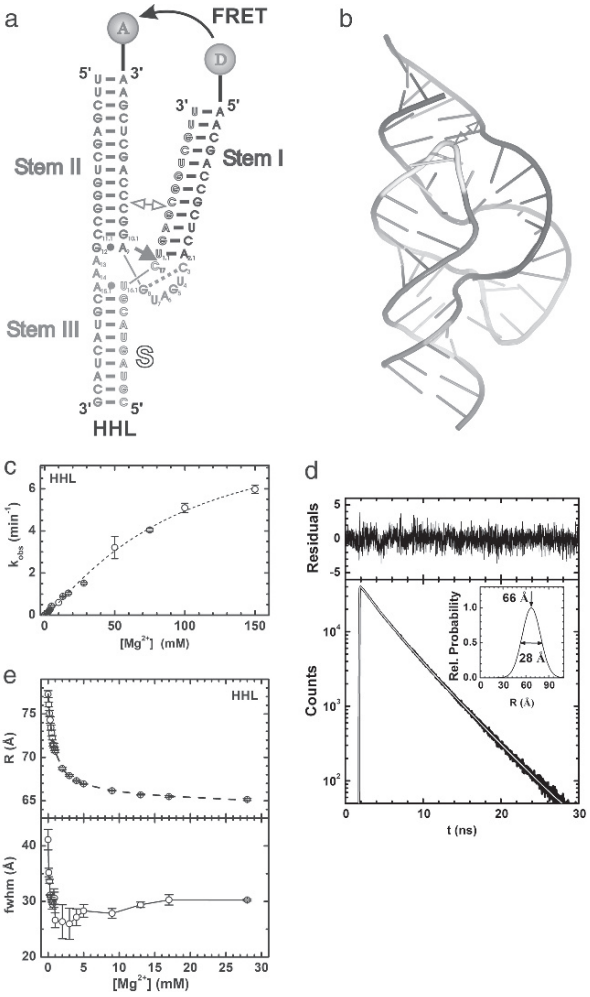

Fig. 5.2 Time-resolved FRET studies of the hammerhead ribozyme. (**a**) Secondary structure of the hammerhead ribozyme HHL utilized in these studies. Helices are color coded, the catalytic core is highlighted in green, and the cleavage site in the substrate (outlined, S) is marked by a closed red arrow. Stems I and II are labeled with donor (D) and acceptor (A) fluorophores, as indicated, which undergo FRET. In extended forms of the ribozyme, Stems I and II interact in the regions marked by an open double-arrow. (**b**) Cartoon representation of the crystal structure of the extended *Schistosoma* hammerhead ribozyme (PDB ID: 2GOZ) (Martick and Scott 2006), color-coded as in panel A except for the silver capping loop that is present only in the extended form. The interaction of an internal and a capping loop in Stems I and II, respectively, is marked by an open double-arrow. (**c**) Mg^{2+} dependence of the observed cleavage rate constant of HHL under standard conditions (50 mM Tris-HCl, pH 8.0, 25°C). (**d**) Representative HHL donor fluorescence decay (bottom, black line) with corresponding fit (white line) in the presence of acceptor under standard conditions with 9 mM Mg^{2+}. Top, fit residuals; inset, resulting single-distance distribution with the indicated mean and fwhm values. (**e**) Mean distance (*top*) and fwhm (*bottom*) of the Stem I–II distance distribution of HHL as a function of Mg^{2+} concentration under standard conditions, as derived by time-resolved FRET analysis similar to panel D. In part modified with permission from (Rueda et al. 2003)

a biophysical technique capable of probing conformational ensembles in solution. FRET, in particular, is a photon-less process that occurs at nanometer distances between a donor (D) fluorophore in the excited electronic state and an acceptor (A) in the ground electronic state. The rate of energy transfer k_T is dependent on the distance r between D and A, as well as the D excited state lifetime τ_D (Lakowicz 2006)

$$k_t(r) = \frac{1}{\tau_D}\left(\frac{R_0}{r}\right)^6$$

The distance R_0 at which the FRET efficiency is 50% is called the Förster distance, after Theodor Förster who first described the theory behind the phenomenon (Förster 1946; Förster 1948). The Förster distance typically ranges from 20 to 70 Å and depends primarily on the spectral overlap of the D emission and A excitation, as well as the relative orientation of the transition dipole moments of the fluorophores. The FRET efficiency is most strongly dependent on the D–A distance around the Förster distance, making it a well suited molecular ruler in biology (Stryer 1978):

$$E_T = \frac{R_0^6}{R_0^6 + r^6}$$

Given the "Y-shaped" structure of the hammerhead ribozyme, its two proximal Stems I and II are suitable placement sites for a D–A pair. Most FRET-based structure probing so far was reported for "minimal" hammerhead ribozyme constructs (Tuschl et al. 1994; Bassi et al. 1997, 1999; Rueda et al. 2003), but their similar global structures and apparent conformational exchange on the local structural level make these studies also relevant to the less studied "extended" versions (Penedo et al. 2004).

A commonly employed "minimal" hammerhead ribozyme termed HHL is shown in Fig. 5.2a. Lilley and co-workers used steady-state FRET (i.e., continuous fluorophore excitation combined with inspection of the emission spectra (Walter 2001, 2002)) to establish that, upon Mg^{2+} titration, two sequential metal ion-induced structural transitions lead to adoption of the "Y-shaped" structure. The first transition leads to coaxial stacking of Stems II and III with an apparent half-titration point for Mg^{2+} of ~0.1 mM, while the second transition presumably organizes the U-turn motif in the catalytic core such that Stems I and II become juxtaposed with an apparent Mg^{2+} half-titration point of ~1 mM (Bassi et al. 1997). In an extended hammerhead ribozyme, these two transitions collapse into a single one at the lower Mg^{2+} concentration (Penedo et al. 2004), suggesting that the loop–loop interactions of the extended hammerhead ribozyme reduce the Mg^{2+}-requirement by an order of magnitude for adopting the Y-shaped structure with folded U-turn of the core.

We utilized the minimal HHL ribozyme to reveal, by combining cleavage assays (Fig. 5.2c) and time-resolved FRET (Figs. 5.2d, e), a third folding transition at even higher Mg^{2+} concentrations (half-titration point of 90 mM), which finally activates the ribozyme (Rueda et al. 2003). For time-resolved FRET we site-specifically labeled Stems I and II with fluorescein donor (D) and tetramethylrhodamine acceptor (A), respectively, as indicated in Fig. 5.2a. To avoid flurophore quenching by adjacent guanines, two A:U base pairs were placed next to the fluorophores at the ends of the labeled stems.

Time-resolved FRET measures the donor fluorescence decay lifetimes (typically on the order of a few nanoseconds) in both a donor-only and a donor-acceptor doubly-labeled sample to derive the fluorophore distance distribution from the relative decay acceleration in the presence of the acceptor (Walter 2001). Relative to the timescale of the donor fluorescence decay, most molecular motions are slow so that time-resolved FRET takes a snapshot of the donor-acceptor distance distribution arising (at least in part) from structural flexibility among the ensemble of molecules in the sample.

Given the placement of the fluorophores in the HHL construct, the mean Stem I–stem II distance and its full width at half-maximum (fwhm) were measured in standard buffer (50 mM Tris-HCl, pH 8.0) at 25°C as a function of Mg^{2+} concentration (Figs. 5.2d, e). A large global structural transition with a Mg^{2+} dissociation constant in the physiological range of ~1 mM was observed which brings Stems I and II closer together and sharpens their distance distribution (i.e., lowers the fwhm) (Fig. 5.2e), essentially consistent with the earlier studies (Bassi et al. 1997; Hammann and Lilley 2002). Na^{+} ions impair this Mg^{2+}-induced transition. However, a previously undetected, relatively subtle global rearrangement coincides with catalytic activation at ~100-fold lower Mg^{2+} affinity. This transition broadens the Stem I–II distance distribution and is not impaired by Na^{+} (Fig. 5.2e). Notably, a catalytically more active hammerhead ribozyme (termed HHα) exhibits the same general behavior with higher Mg^{2+} affinity and a larger fwhm than HHL, further supporting the notion that a shortening of the mean Stem I–II distance combined with larger flexibility at high Mg^{2+}-concentrations is important for catalysis (Rueda et al. 2003).

5.4 The Hairpin Ribozyme

The hairpin ribozyme is derived from the negative-polarity strand of the satellite RNA associated with the tobacco ringspot virus, where it complements a hammerhead ribozyme motif in the positive-polarity strand to affect double-rolling circle replication of the satellite (Haseloff and Gerlach 1989; Feldstein et al. 1990; Walter and Burke 1998). A minimal hairpin ribozyme of ~50 nucleotides can be segmented into two separate strands (termed RzA and RzB) that bind a substrate to form domain A, comprising helices H1 and H2 and the symmetric internal loop A (Fig. 5.3a). Domain A is connected by a flexible hinge to domain B, which comprises

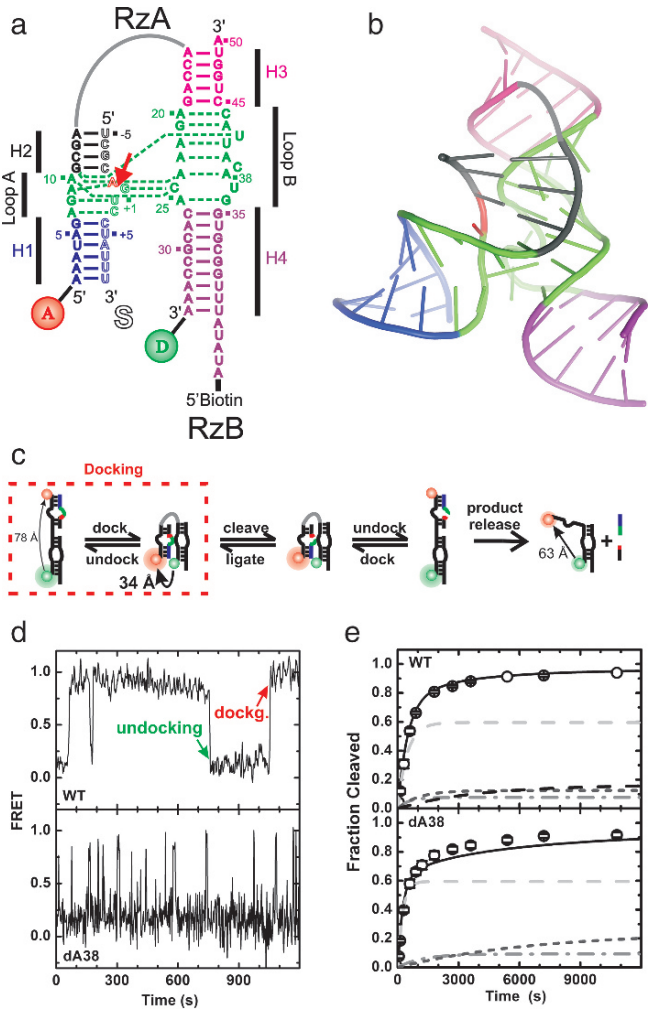

Fig. 5.3 Steady-state FRET studies of the hairpin ribozyme. (**a**) Secondary structure of the hairpin ribozyme from the tobacco ringspot satellite RNA utilized in these studies. Helices are color coded, the catalytic core is highlighted in green, and the cleavage site in the substrate (outlined, S) is marked by a closed red arrow. The RzA strand is labeled with donor (D) and acceptor (A) fluorophores, as indicated, which undergo FRET. (**b**) Cartoon representation of the crystal structure of a junctionless, all-RNA hairpin ribozyme (PDB ID: 2OUE) (Salter et al. 2006), color-coded as in panel A; a gray line was added to indicate the connectivity of the two domains. (**c**) Reaction pathway of the hairpin ribozyme as revealed by ensemble and single molecule FRET. Fluorophore distances measured by time-resolved FRET are indicated. (**d**) Representative single molecule FRET time trace of wild-type (WT) and dA38 mutant ribozymes after binding of non-cleavable (2′-OMe-A_{-1}) substrate analog under standard conditions (50 mM Tris-HCl, pH 7.5, 12 mM Mg^{2+}, 25°C). One undocking and one docking event are indicated. (**e**) Experimental (symbols) and simulated (lines) cleavage time courses of the WT and dA38 mutant ribozymes under standard conditions. The predicted contributions from four and three experimentally detected molecule sub-populations, respectively, are indicated by gray and dashed lines. In part modified with permission from (Rueda et al. 2004) (See figure insert for color reproduction)

H3 and H4 and the asymmetric internal loop B. Site-specific cleavage and ligation occur in the substrate strand of domain A (Fig. 5.3a) and require the presence of either millimolar concentrations of divalent or molar concentrations of monovalent cations (Hampel and Cowan 1997; Nesbitt et al. 1997; Young et al. 1997; Murray et al. 1998). A number of crystal structures have highlighted the intricate network of hydrogen bonding and stacking interactions that docks loops A and B to form the catalytic core, and single out a specific phosphodiester bond for cleavage (Fig. 5.3b) (Rupert and Ferre-D'Amare 2001; Rupert et al. 2002; Alam et al. 2005; Salter et al. 2006; Torelli et al. 2007), presumably involving (electrostatic) transition state stabilization (Rupert et al. 2002; Kuzmin et al. 2004; Kuzmin et al. 2005) and/or general acid–base catalysis by RNA functional groups of A38 and perhaps G8 (Pinard et al. 2001; Bevilacqua 2003; Wilson et al. 2006) and/or structural water molecules (Rhodes et al. 2006; Torelli et al. 2007).

To dissect steps on the reaction pathway of the hairpin ribozyme, the ensemble relaxation kinetics from the undocked to the docked conformational state upon substrate addition were monitored by steady-state FRET between domain-terminal fluorophores (Walter et al. 1998c). The results revealed that substrate binding (secondary structure formation) and domain docking (tertiary structure formation) are two distinct steps on the reaction pathway. Upon docking, the ribozyme reversibly cleaves the substrate, followed by undocking and product release (Fig. 5.3c). Docking of domains A and B, as monitored by FRET, is thus required and at least partially rate-limiting for both cleavage and ligation. Ensemble steady-state FRET assays also revealed that most modifications to the RNA, or reaction conditions known to inhibit catalysis do in fact prevent the necessary domain docking (Walter et al. 1998c).

To further characterize the folding intermediates, the undocked and docked conformers of the hairpin ribozyme were examined under varying Mg^{2+} concentrations by time-resolved FRET (Walter et al. 1999). This analysis yielded the interdomain distance distributions, their mean distances, and their fractional contributions, which define differences in docking free energy. The catalytically active tertiary structure was found to be stabilized by both specific docking interactions between domains A and B and the topology of the intervening helical junction. In particular, at near-physiological Mg^{2+} concentrations, the naturally occurring four-way junction thermodynamically favors docking, whereas a nicked or connected two-way junction and a three-way junction favor the undocked conformer. These findings highlighted the importance of the four-way junction as part of the hairpin ribozyme motif found in the satellite RNA to bring domains A and B into proximity, independent of specific docking interactions between them (Walter et al. 1999). This view is qualitatively supported by ensemble steady-state FRET assays (Murchie et al. 1998; Walter et al. 1998a, b).

Over the past few years, single molecule FRET has become increasingly popular for illuminating pathways of RNA folding and catalysis (Zhuang 2005; Ditzler et al. 2007). Using prism-based total internal reflection fluorescence microscopy (TIRFM) (Walter et al. 2008), low background noise levels can be obtained during the observation of single, surface immobilized hairpin ribozyme molecules that

reproduce the catalytic rate constants of free solution conditions (Zhuang et al. 2002). Since single molecules exist in either the undocked or the docked conformation, single molecule FRET can detect (given sufficient time resolution) individual transitions between the two states (Fig. 5.3d). Statistics of the dwell or residency times in a specific state then yield the kinetics associated with the inter-conversion of states (Zhuang et al. 2002; Ditzler et al. 2007), unlike in ensemble behavior where the individual molecule behavior is averaged out and only non-equilibrium relaxation kinetics can be measured.

Three single molecule FRET approaches have been used to dissect the reaction pathway of two- and four-way hairpin ribozymes (Fig. 5.3c). They provide access to the chemical turnover rates (Ditzler et al. 2007): (i) Probing of inactivated ribozyme-substrate and -product complexes in combination with ensemble activity assays and mechanistic modeling (Rueda et al. 2004). This approach depends on the accuracy of assumptions necessary for the kinetic modeling, such as that of identical folding behavior of the inactivated and active ribozyme complexes. (ii) Direct observation of catalytic turnover due to associated changes in FRET or dwell time constant (Nahas et al. 2004). This approach depends on the ability to clearly distinguish such changes from unrelated fluctuations. (iii) Indirect observation of the probability for catalytic events using a succession of buffer exchanges to produce distinct time sequences of the single molecule FRET signal that serve as kinetic "fingerprints" of specific catalytic intermediates (Liu et al. 2007). This approach requires a very careful "sorting" of the resulting time traces by behavioral classes.

These three approaches showed that the rate of substrate cleavage is rate-limited by a combination of conformational transitions and reversible chemical equilibrium (Zhuang et al. 2002; Rueda et al. 2004). Adoption of the four-way junction and shortening of the substrate accelerate docking and product dissociation, respectively, shifting the rate limitation largely toward reaction chemistry (Nahas et al. 2004). Strikingly, all studies consistently found evidence for non-interchanging sub-populations of the hairpin ribozyme that are readily distinguished by their dwell time in the docked state (Fig. 5.3d) (Zhuang et al. 2002; Bokinsky et al. 2003; Nahas et al. 2004; Okumus et al. 2004; Rueda et al. 2004; Liu et al. 2007). These complex structural dynamics quantitatively explains the heterogeneous cleavage kinetics common to many catalytic RNAs (Zhuang et al. 2002; Rueda et al. 2004), as evident from the fact that only the sum of the predicted contributions of each sub-population can fully reproduce the biphasic kinetics of product formation. Figure 5.3e illustrates this point on exemplary wild-type (WT) and dA38 mutant cleavage time courses.

These observations suggest that single molecule approaches are critical in delineating the complexities of RNA folding and function (Zhuang 2005; Ditzler et al. 2007). Furthermore, in conjunction with site-specific mutations, metal ion titrations, and computational modeling they reveal that the domains of the hairpin ribozyme are in near-contact in the docking transition state even though the native tertiary contacts are at most partially formed (Bokinsky et al. 2003). More in-depth single molecule FRET analysis indicate that most site-specific RNA modifications

affect the rate constants of docking, undocking, and chemistry even when they are distant from any direct docking and catalytic interactions (Rueda et al. 2004). This effect is likely due to a long-range network of hydrogen bonding and stacking interactions that involves several structural water molecules in the catalytic core (Rhodes et al. 2006; Walter 2007).

5.5 The HDV Ribozyme

The hepatitis delta virus (HDV) is a human pathogen and satellite of the hepatitis B virus; co-infection with both leads to enhanced liver damage. HDV contains a viroid-like genomic RNA that is thought to undergo replication via a double rolling-circle mechanism wherein both the genomic and anti-genomic RNAs self-cleave and re-ligate into circular monomers (Taylor 2006). The cleavage activities map to ~85-nucleotide RNA motifs, the genomic and anti-genomic ribozymes, that have ~75% sequence homology and share a common secondary and tertiary structure (Been 2006). The HDV ribozyme is comprised of five helices P1, P1.1, P2, P3, and P4 that are tight-knit into a double-nested pseudoknot (Fig. 5.4a) (Perrotta and Been 1991; Ferre-D'Amare et al. 1998), making this fold thermodynamically highly stable, perhaps as an adaptation to the conditions in mammalian cells (Perrotta and Been 1991). A structurally and biochemically closely related ribozyme motif of unknown biological function resides in an intron of the human *CPEB3* gene, suggesting that HDV may have parasitically arisen from the human transcriptome (Salehi-Ashtiani et al. 2006).

The cleavage site of the HDV ribozyme is located at the junction of a single-stranded 5′-sequence and the G1:U37 wobble pair that closes the P1 helix (Fig. 5.4a). The HDV ribozyme was the first (and arguably is still the clearest) example of an RNA enzyme where structural and kinetic data suggest a specific role for an RNA side chain in catalysis; the exact nature of this role however remains controversial. In particular, two kinetically equivalent roles – those of general base and general acid catalyst – have been alternatively proposed for nucleobase C75 in the genomic ribozyme (or the equivalent C76 in the antigenomic form) (Perrotta et al. 1999; Nakano et al. 2000; Ke et al. 2004; Das 2005).

The crystal structures of the reaction precursor and product show that C75 is jutting from its location in the joiner between helices P4 and P2 (J4/2) toward the cleavage site (Ferre-D'Amare et al. 1998; Ferre-D'Amare and Doudna 2000; Ke et al. 2004) (Fig. 5.4b). Controversially, the conformation of the catalytic pocket in the precursor crystal led to a model of general base involvement of C75 in the reaction mechanism (Ke et al. 2004), while the hydrogen bond between C75(N3) and the 5′-OH leaving group in the product crystal (Ferre-D'Amare et al. 1998; Ferre-D'Amare and Doudna 2000) is suggestive of general acid catalysis. ^{13}C-NMR spectroscopy yielded no clear evidence for the significant pK_a shift expected for C75(N3) to play a direct role in catalysis (Luptak et al. 2001), whereas a recent Raman crystallography approach did (Gong et al. 2007). A hydrated Mg^{2+} ion,

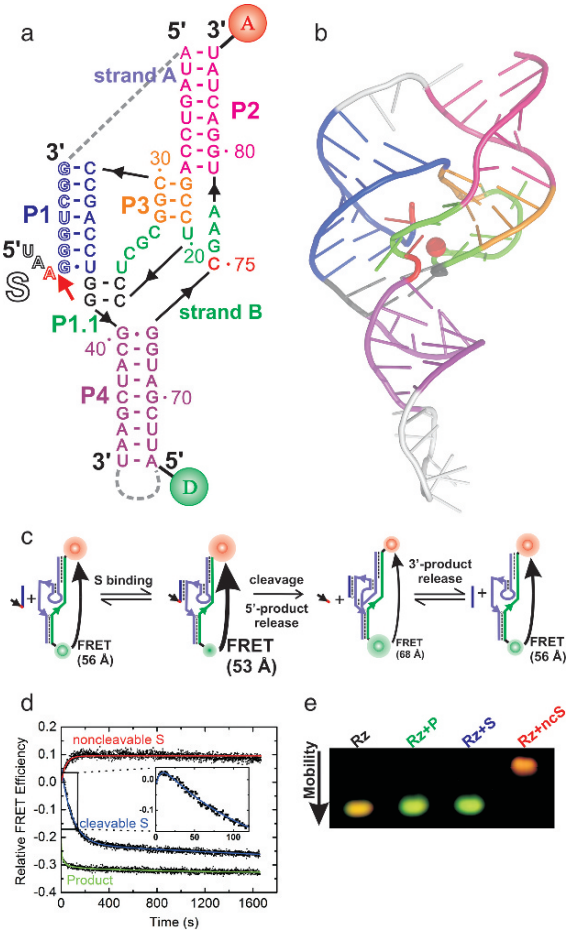

Fig. 5.4 FRET studies of the HDV ribozyme. (**a**) Secondary structure of the HDV ribozyme D1 utilized in these studies. Helices are color coded, the catalytic core is highlighted in green, and the cleavage site in the substrate (outlined, S) is marked by a closed red arrow. Strand B of the ribozyme is labeled with donor (D) and acceptor (A) fluorophores, as indicated, which undergo FRET. Dashed gray lines indicate connections that are present in the naturally occurring, cis-acting, genomic and antigenomic HDV ribozymes. (**b**) Cartoon representation of the crystal structure of the genomic HDV ribozyme (PDB ID: 1SJ3) (Ke et al. 2004), color-coded as in panel A with connections removed for the trans-acting D1 construct shown in silver. Red sphere, presumably catalytically involved Mg^{2+} ion. (**c**) Reaction pathway of the HDV ribozyme as revealed by ensemble steady-state FRET. Fluorophore distances measured by time-resolved FRET are indicated. (**d**) Relative FRET efficiency (calculated as ratio of the acceptor:donor fluorescence signals) over time of the doubly labeled D1 construct upon addition of a fivefold excess of non-cleavable substrate analogue (ncS3), cleavable substrate (S3; which binds, leading to an increase [inset], followed by a decrease upon cleavage), or 3′ product (3′P), as indicated, under standard conditions (40 mM Tris-HCl, pH 7.5, 11 mM Mg^{2+}, 25 mM DTT, 25°C). (**e**) Non-denaturing gel electrophoresis of the doubly labeled ribozyme alone (Rz) and in complex with 3′-product (Rz + P), cleavable substrate (Rz + S; this complex undergoes catalysis and is indistinguishable from the 3′-product complex), and non-cleavable substrate (Rz + ncS), as indicated. Detection is by FRET in the gel. In part modified with permission from (Pereira et al. 2002) (See figure insert for color reproduction)

located near the cleavage site (Ke et al. 2004) is, while not absolutely obligatory for activity (Nakano et al. 2003), thought to assist C75 by providing the complementary function in general acid–base catalysis (Nakano et al. 2000; Nakano and Bevilacqua 2007). However, it has been difficult to discern by either mechanistic or structural studies which specific role is played by these two components (Bevilacqua and Yajima 2006).

Studies of the HDV ribozyme mechanism are complicated by the fact that a conformational change accompanies catalysis (Fig. 5.4c). Probing a synthetic three-strand form (Fig. 5.4a) by a combination of steady-state FRET (Fig. 5.4d), time-resolved FRET, and electrophoretic mobility shift FRET assays (Fig. 5.4e) revealed that the distance between the P2 and P4 termini is significantly shorter (by ~15 Å) in the reaction precursor than in the product (Pereira et al. 2002). Complementary assays based on 2-aminopurine fluorescence (Harris et al. 2002) and terbium(III)-mediated footprinting (Jeong et al. 2003) highlighted local conformational changes that accompany the global conformational change detected by FRET. Subsequently, the crystal structure of the genomic HDV ribozyme precursor (Ke et al. 2004) showed a similar, if less pronounced P2–P4 contraction relative to the product structure (Ferre-D'Amare et al. 1998), validating the FRET observations on the three-strand form. Time-resolved FRET studies of the latter RNA in dependence of Mg^{2+} found that the precursor shortens while the product expands with increasing divalent metal ion concentration, thereby amplifying the structural differences observed in the crystal structures (Tinsley et al. 2004). Such amplification of the conformational change may contribute to systematically lower cleavage rate constants observed for multi-strand ("trans-acting") constructs relative to the contiguous ("cis-acting") genomic and anti- genomic HDV ribozymes (Tinsley and Walter 2007). Finally, the Mg^{2+} affinity of the C75 wild-type as monitored by time-resolved FRET is slightly (~2-fold) lower than that of a C75U mutant, consistent with the notion that C75 binds in proximity to and competes with a divalent metal ion (Tinsley et al. 2004), as also suggested by X-ray crystallography (Ke et al. 2004) and mechanistic studies (Nakano et al. 2000).

5.6 The VS Ribozyme

The Varkud Satellite (VS) RNA is located within the mitochondria of the bread mold *Neurospora*, where it replicates a retrotransposon by reverse transcription into a (circular) DNA plasmid, transcription into multimeric VS RNA copies, and self-cleavage and re-ligation back into circular, monomeric VS RNA (Collins and Saville 1990; Saville and Collins 1990). The VS ribozyme is the largest and most complex of the small ribozymes, and accordingly, least structurally understood. The secondary structure of the VS ribozyme consists of six helical segments: Stem-loop I forms the substrate domain with the cleavage site and stem-loops II through VI comprising the catalytic domain. The catalytic domain is organized into two three-way junctions (II-III-VI) and (III-IV-V) that share helix III (Fig. 5.5a). It recognizes the substrate predominantly through tertiary interactions, particularly the

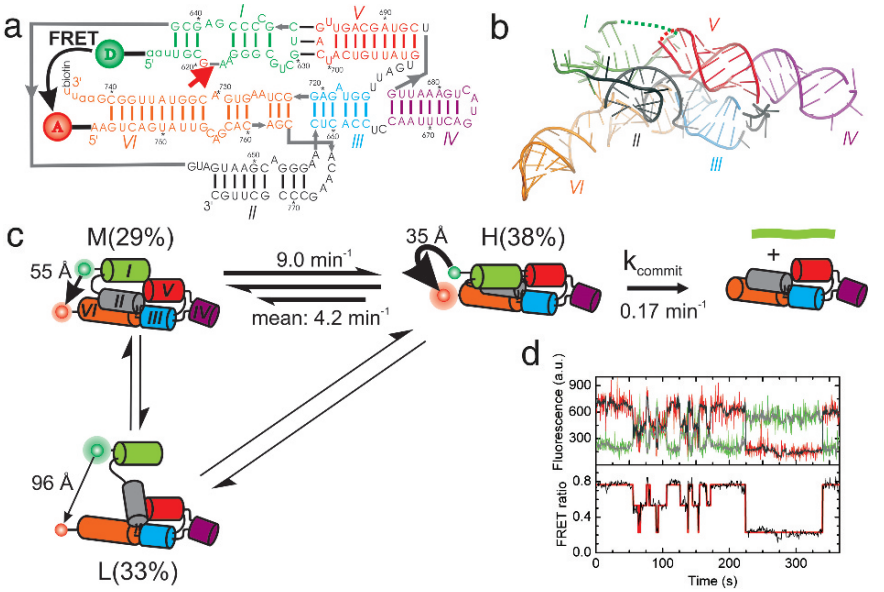

Fig. 5.5 Single molecule FRET studies of the VS ribozyme. (**a**) Secondary structure of the VS ribozyme G11 utilized in these studies. Helices are color coded, the cleavage site is marked with a closed red arrow, and the FRET donor (D) and acceptor (A) and biotin labeling sites are indicated. (**b**) Tertiary structure model of the VS ribozyme, using the same color code as in panel A. Some strand connectivities are incomplete in the model; the ones in the I–V kissing loop are indicated by dashed lines. (**c**) Structural and kinetic model of the reaction pathway of the WT VS ribozyme as derived from single molecule FRET. The helix colors match those in panel A. (**d**) Single molecule FRET time trace of a VS ribozyme (Hiley and Collins 2001). The raw Cy3 donor and Cy5 acceptor fluorescence signals are green and red, respectively (upper panel). Superimposed in gray are the data after applying a non-linear filter (Haran 2004). The FRET ratio (lower panel, black trace) is calculated from the filtered data as acceptor/(donor + acceptor) and reveals three distinct states by Hidden Markov modeling (red line). In part modified with permission from (Pereira et al. 2008) (See figure insert for color reproduction)

Mg^{2+}-dependent kissing-loop interaction between stems I and V (Rastogi et al. 1996; Andersen and Collins 2000). This exposes the substrate to the catalytic core around the 730 loop of helix VI (Hiley et al. 2002) (Fig. 5.5a), wherein functional groups of G638 and A756 appear to be involved in catalysis (Wilson et al. 2007; Jaikaran et al. 2008). Cleavage activity is observed in the absence of divalent metal ions, consistent with the sufficiency of RNA residues for catalysis (Murray et al. 1998). Models of the global fold of the VS ribozyme have been derived from ensemble steady-state FRET of the isolated three-way junctions (Lafontaine et al. 2001, 2002), mutagenesis, native gel electrophoresis, hydroxyl radical foot printing, and UV-induced cross linking (Beattie et al. 1995; Hiley and Collins 2001; Hiley et al. 2002).

To assess the folding dynamics of the VS ribozyme, single molecule FRET was performed on the well-studied G11 construct (Pereira et al. 2008). The 5′ end of

G11 was labeled with a Cy3 FRET donor by a ligation approach, while the non-essential closing loop of helix VI was opened to attach a 5′-Cy5 FRET acceptor and a 3′-biotin for surface immobilization. This wild-type construct is designed to monitor global distance changes between the substrate stem-loop I and the catalytic core in helix VI (Fig. 5.5a). It exhibits dynamic three-state folding, where especially a mid (M) and high FRET (H) state inter-convert with rapid and heterogeneous kinetics (Fig. 5.5c), showing occasional excursions into a long-lived low FRET (L) state (Fig. 5.5d). Disruption of the kissing-loop interaction upon mutation of a single base pair completely eliminates both the H state and catalytic activity, while a second-site mutation to invert the base pair restores both, suggesting that the H state is required for catalytic activity (Pereira et al. 2008). Kinetic modeling showed, however, that formation of the H state is not rate-limiting, suggesting that a slow and local conformational change, hidden from FRET observation, must be traversed before the ribozyme undergoes self-cleavage (Pereira et al. 2008).

Mutation of the II–III–VI junction leads to reduced catalytic activity as a consequence of less frequent H state access, suggesting that the II–III–VI junction acts as an important structural scaffold onto which the I–V kissing-loop interaction is built. These observations provide evidence for hierarchical folding of the VS ribozyme as an example of a more complex ribozyme with multiple structural motifs (Pereira et al. 2008). Notably, a change in topology that connects stem-loop I with the 3′- rather than the 5′-end of the catalytic core leads to considerably faster cleavage activity, ratelimited by proton transfer (Smith and Collins 2007), and more rapid and stable docking into the high FRET state (Pereira et al. 2008).

5.7 The *glmS* Ribozyme

A recently discovered class of gene regulatory RNAs, termed riboswitches, are commonly found in the 5′-untranslated regions of mRNAs in Gram-positive bacteria such as *Bacillus*, where they typically change conformation upon binding a specific metabolite, thus refolding an adjacent expression platform that may be sometimes up or down – and which regulates expression of the downstream gene involved in biosynthesis or transport of the metabolite (Winkler and Breaker 2005; Coppins et al. 2007; Edwards et al. 2007; Al-Hashimi and Walter 2008) (please note that riboswitches are the focus of the accompanying chapters by Batey and Schwalbe and coworkers). Given that riboswitches are mostly bacterial, highly selective receptors for small, drug-like metabolites, they may represent a new class of RNA targets for the development of antibiotics (Blount and Breaker 2006).

The riboswitch known as the *glmS* ribozyme is unique in that binding of its ligand glucosamine-6-phosphate (GlcN6P) induces self-cleavage (Winkler et al. 2004) and subsequent intracellular degradation of the embedding *glmS* mRNA, which encodes GlcN6P synthase (Collins et al. 2007). While ligand is absolutely required for catalytic activity and specificity for GlcN6P is high, several structurally related

amine-containing compounds were found to partially activate the riboswitch, suggesting that the aminogroup participates in general acid–base catalysis rather than functions as an allosteric activator (McCarthy et al. 2005). Crystal structures of the *glmS* ribozyme (Figs. 5.6a, b) revealed three parallel helical stacks with a doubly pseudo knotted core that binds GlcN6P in a manner consistent with general acid–base catalysis by GlcN6P, in conjunction with G40 of the ribozyme and possibly structural water molecules (Klein and Ferre-D'Amare 2006; Cochrane et al. 2007; Walter 2007). Notably, the *glmS* ribozyme can fold and function in the absence of divalent metal ions (Roth et al. 2006).

To address with maximal sensitivity the question of whether any conformational rearrangements accompany ligand binding by the *glmS* ribozyme, the closing loop of P1 was removed to obtain a trans-acting ribozyme with external substrate for

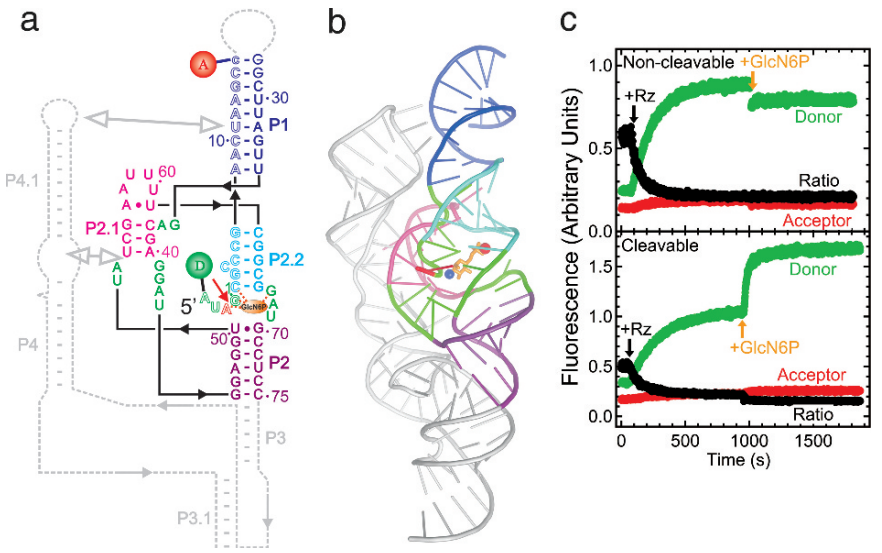

Fig. 5.6 Steady-state FRET studies of the *glmS* ribozyme. (**a**) Secondary structure of the trans-acting *glmS* ribozyme utilized in these studies. Helices are color coded, the catalytic core is highlighted in green, the cleavage site in the substrate (outlined, S) is marked by a closed red arrow, and the cofactor GlcN6P is shown as an orange oval interacting with several core residues (dashed orange lines). The substrate strand is labeled with donor (D) and acceptor (A) fluorophores, as indicated, which undergo FRET. Dashed gray lines indicate connections and a downstream pseudoknot that are present in the naturally occurring, cis-acting ribozyme. (**b**) Cartoon representation of the crystal structure of the *Thermoanaerobacter tengcongensis glmS* ribozyme (PDB ID: 2H0Z) (Klein and Ferre-D'Amare 2006), color-coded as in panel A with removed parts shown in silver. Red sphere, ligand-chelating Mg^{2+} ion; blue sphere, amino group of the ligand presumably involved in catalysis. (**c**) Changes over time in donor, acceptor, and acceptor:donor ratio signals upon addition of a tenfold excess of *glmS* ribozyme (Rz) and subsequently saturating (10 mM) GlcN6P ligand to either the non-cleavable or cleavable substrate under standard conditions (50 mM HEPES-KOH, pH 7.5, 200 mM K^+, 10 mM Mg^{2+}, 25 mM DTT, 25°C), as indicated. In part modified with permission from (Tinsley et al. 2007) (See figure insert for color reproduction)

FRET labeling, while the downstream P3–P4.1 was truncated to obtain a minimal, slightly destabilized ribozyme core (Tinsley et al. 2007) (Figs. 5.6a, b). Fluorescein donor and tetramethylrhodamine acceptor fluorophores were attached to the substrate 5′- and 3′-termini, respectively, to detect changes in distance along the central P1:P2.2 helical axis that encompasses the GlcN6P binding and cleavage sites.

Addition of an excess of ribozyme to the FRET labeled non-cleavable substrate analog resulted in a significant increase in donor fluorescence and corresponding decrease in acceptor:donor signal ratio (Fig. 5.6c top). These changes are expected as the binding of the ribozyme will cause an extension of the initially random-coil substrate in the complex. Upon further addition of 10 mM GlcN6P, however, no significant changes in fluorescence signal and FRET efficiency were observed (Fig. 5.6c top). By contrast, a considerable increase in donor signal and resulting decrease in FRET efficiency were evident upon addition of the GlcN6P ligand to the ribozyme-cleavable substrate complex (Fig. 5.6c bottom), as expected from ligand-induced substrate cleavage and dissociation of the 5′-product with attached donor fluorophore. These results are corroborated by time-resolved FRET analysis, where the donor-acceptor distance in the absence and presence of GlcN6P was both found to be 52 Å (Tinsley et al. 2007). Taken together, these results support the notion that the *glmS* ribozyme is fully folded in solution prior to binding its activating ligand (cofactor), which is consistent with precursor and product crystal structures (Klein and Ferre-D'Amare 2006; Cochrane et al. 2007) and observations from hydroxyl radical foot printing in solution (Hampel and Tinsley 2006).

5.8 Common and Diverse Features: Attaining Site-Specificity in Cleavage

The RNA backbone can spontaneously undergo acid-base catalyzed self-cleavage via the same reaction chemistry utilized by the small ribozymes (Fig. 5.1). Under physiologic conditions, spontaneous RNA degradation occurs at a rate constant estimated to average ~10^{-7} min^{-1} per bond (Emilsson et al. 2003), with a strong dependence on both sequence and structure context (Kaukinen et al. 2002). In double-stranded (Watson–Crick base paired) RNA, the angle between the 2′O-P-5′O atoms is 65–70°, which is significantly different from the optimal angle for in-line attack of close to 180° (Min et al. 2007). This renders the backbone of double-stranded RNA chemically quite inert. Strikingly, all crystal structures of small ribozymes that are thought to be catalytically relevant find the cleavage site in a partially not Watson–Crick paired (or single-stranded) RNA segment featuring a backbone kink (Rupert and Ferre-D'Amare 2001; Ke et al. 2004; Klein and Ferre-D'Amare 2006; Martick and Scott 2006). In fact, the absence of such a backbone kink was used as an indication that the early crystal structures of the hammerhead ribozyme could only be activated by a conformational change after which the cleavage site would adopt non-double-helical characteristics (Wedekind and McKay 1998; Blount and Uhlenbeck 2005).

The small ribozymes have evolved in a convergent manner to prepare a specific bond for a common reaction chemistry, and while they utilize different strategies and structural contexts, in all cases the two nucleotides immediately upstream and downstream of the scissile phosphate are splayed apart in distinct hydrogen bonding and stacking interactions, enforcing unusual torsion angles that kink the backbone (Sefcikova et al. 2007; Walter 2007). Estimates suggest that adoption of an ideal in-line attack configuration accelerates spontaneous backbone cleavage only by <100-fold (Emilsson et al. 2003; Min et al. 2007), supporting the notion that backbone kinking is likely to serve more than one role: to facilitate in-line attack, to specify a bond near the kink for cleavage by exposure to the general acid and base that affect catalysis, and to destabilize the ground state structure (Fig. 5.1).

Specific nucleo bases, structural water molecules, and – in the case of the HDV ribozyme – a hydrated divalent metal ion are generally proximal to the exposed scissile phosphate of the small ribozymes, placed there by the intricacies of the global and local RNA fold. The nucleo bases so far implicated in general acid–base (or electrostatic) catalysis are mostly the purines G and A, perhaps due to the larger number of their functional groups and more extended aromatic system with larger surface area for stacking. The only exception to this rule is the HDV ribozyme that utilizes a cytosine (C75) for catalysis and is, perhaps not coincidentally, also the only small ribozyme strongly dependent on divalent metal ions for activity (Murray et al. 1998). This and other roles of metal ions are the focus of the following segment.

5.9 Common and Diverse Features: The Roles of Metal Ions

All small ribozymes show at least residual catalytic function in the complete absence of divalent metal ions, as long as sufficient countercharge in the form of monovalents is provided to neutralize the negatively charged sugar–phosphate backbone (Hampel and Cowan 1997; Nesbitt et al. 1997; Young et al. 1997; Murray et al. 1998; Nakano et al. 2000, 2003; Curtis and Bartel 2001; O'Rear et al. 2001; Roth et al. 2006). This observation contrasts with ribozymes catalyzing more complex phosphodiester transfers, which consistently appear to require a pair of Mg^{2+} ions for catalysis (Walter 2007) (see also accompanying chapters by Woodson, Pyle, and Harris and coworkers). The simpler chemistry executed by the small ribozymes typically requires neither an external nucleophile (as do most larger ribozymes) nor an external catalytic cofactor (except perhaps for ubiquitous water molecules), making small ribozymes surprisingly self-sufficient and versatile, perhaps as an adaptation to their function in parasite replication. Exceptions are the *glmS* ribozyme, which requires GlcN6P as a cofactor and is not a parasite-derived ribozyme but is embedded in bacterial mRNA to control gene expression (Winkler et al. 2004), and the HDV ribozyme, which not only is part of the HDV viroid but is also embedded in the human genome (Salehi-Ashtiani et al. 2006).

The role of metal ions in folding of the small ribozymes is much more unequivocal, especially under physiologic (low-ionic strength) conditions, where Mg^{2+} is the

preferred, highest-affinity folding cofactor. Mg^{2+} is thought to bind RNA in three different modes, by specific inner-sphere coordination (chelation), by outer-sphere binding where a single water layer influences the ion position through steric packing and hydrogen bonding, and by diffuse association with the long-range RNA electrostatic field through multiple water layers (Draper et al. 2005). FRET studies have shown that tertiary structure folding is generally accelerated (and thermodynamically stabilized) and unfolding decelerated by increasing Mg^{2+} concentrations, although differential saturation behavior of the two Mg^{2+} dependency curves is observed for the hairpin ribozyme (Bokinsky et al. 2003). Resulting modeling studies interpret this behavior as an indication that the folding transition state is compacted by Mg^{2+}-based bridging of the two ribozyme domains, even before tertiary hydrogen bond and stacking interactions are extensively formed (Bokinsky et al. 2003). How general this behavior is for the small ribozymes remains to be seen.

5.10 Common and Diverse Features: RNA Structural Dynamics

The catalytic transition state of any enzyme is, by definition, a high-energy state along the reaction pathway that only exists on the timescale of a bond vibration. By contrast, structures observed in a crystalline and solution state by, for example, X-ray crystallography and NMR, respectively, are ensemble-averaged, low-energy ground states, even if perturbed by employing transition state analogs. As a consequence, the available high-resolution crystal structures of ribozymes need to be animated with their dynamics to understand the inherently dynamic processes underlying catalysis.

Ensemble and single molecule FRET has extensively contributed to our understanding of how and why the small ribozymes fold or show intrinsic dynamics. With one exception, global structural changes that rearrange helical alignments for catalytic activation (as in the hammerhead ribozyme), "dock" substrate and catalytic core domains (as in the hairpin and VS ribozymes), or accompany and possibly control catalysis (as in the HDV ribozyme) have readily been detected by FRET in all small ribozymes. It is tempting to speculate that such large-scale conformational rearrangements from inactive to active states serve a biological role by controlling the activity of the catalytic motif during satellite replication in dependence of intracellular cues. Notably, the *glmS* ribozyme is devoid of any such significant conformational change, but is catalytically triggered by a different kind of intracellular cue in the form of a threshold concentration of its catalytic cofactor GlcN6P.

Protein enzymes are thought to exploit a global network of coupled molecular motions to facilitate the chemical reaction they catalyze. This network comprises fast thermal motions that are at equilibrium while the reaction progresses along the reaction pathway; and these motions lead to slower, larger-scale conformational changes that directly facilitate reaction chemistry (Hammes-Schiffer and Benkovic 2006). Whether ribozymes employ a similar strategy to accelerate catalysis is not known, but single molecule FRET probing in combination with molecular dynamics

simulations has revealed that at least the hairpin ribozyme exhibits analogous networks of coupled molecular motions throughout its catalytic core (Rueda et al. 2004; Rhodes et al. 2006). Reaction chemistry in an enzymatic reaction is largely of a local nature, suggesting that the dynamics contributing directly to catalysis in RNA would mostly entail vibrations, torsional librations, sugar re-puckering, and longitudinal and lateral motions of bases, all of which take place in the tens-of-femtoseconds to low-nanosecond time regime (Al-Hashimi and Walter 2008). It remains to be determined whether global structural changes at the nanosecond to minute timescale, as observable by FRET, couple with these local dynamics and contribute to the catalytic power of the small ribozymes.

In conclusion, many common features are emerging from a comparison of the five naturally occurring, structurally very distinct small ribozymes. Diverseness between them probably highlights evolutionary adaptation to specific functional requirements. Future studies using FRET and other biophysical techniques promise to elucidate more about the fundamental principles underlying RNA catalysis, enabling an even broader comparison of enzymes, including those based on protein, and a potential utilization in human technology.

References

Al-Hashimi HM, Walter NG (2008) RNA dynamics: it's about time. Curr Opin Struct Biol 18:321–329

Alam S, Grum-Tokars V, Krucinska J, Kundracik ML, Wedekind JE (2005) Conformational heterogeneity at position U37 of an all-RNA hairpin ribozyme with implications for metal binding and the catalytic structure of the S-turn. Biochemistry 44:14396–14408

Andersen AA, Collins RA (2000) Rearrangement of a stable RNA secondary structure during VS ribozyme catalysis. Mol Cell 5:469–478

Bassi GS, Murchie AI, Walter F, Clegg RM, Lilley DM (1997) Ion-induced folding of the hammerhead ribozyme: a fluorescence resonance energy transfer study. EMBO J 16:7481–7489

Bassi GS, Mollegaard NE, Murchie AI, Lilley DM (1999) RNA folding and misfolding of the hammerhead ribozyme. Biochemistry 38:3345–3354

Beattie TL, Olive JE, Collins RA (1995) A secondary-structure model for the self-cleaving region of Neurospora VS RNA. Proc Natl Acad Sci U S A 92:4686–4690

Been MD (2006) HDV ribozymes. Curr Top Microbiol Immunol 307:47–65

Bevilacqua PC (2003) Mechanistic considerations for general acid-base catalysis by RNA: revisiting the mechanism of the hairpin ribozyme. Biochemistry 42:2259–2265

Bevilacqua PC, Yajima R (2006) Nucleobase catalysis in ribozyme mechanism. Curr Opin Chem Biol 10:455–464

Blount KF, Breaker RR (2006) Riboswitches as antibacterial drug targets. Nat Biotechnol 24:1558–1564

Blount KF, Uhlenbeck OC (2005) The structure-function dilemma of the hammerhead ribozyme. Annu Rev Biophys Biomol Struct 34:415–440

Bokinsky G, Rueda D, Misra VK, Rhodes MM, Gordus A, Babcock HP, Walter NG, Zhuang X (2003) Single-molecule transition-state analysis of RNA folding. Proc Natl Acad Sci U S A 100:9302–9307

Bondensgaard K, Mollova ET, Pardi A (2002) The global conformation of the hammerhead ribozyme determined using residual dipolar couplings. Biochemistry 41:11532–11542

Cochrane JC, Lipchock SV, Strobel SA (2007) Structural investigation of the GlmS ribozyme bound to its catalytic cofactor. Chem Biol 14:97–105
Collins RA, Saville BJ (1990) Independent transfer of mitochondrial chromosomes and plasmids during unstable vegetative fusion in Neurospora. Nature 345:177–179
Collins JA, Irnov I, Baker S, Winkler WC (2007) Mechanism of mRNA destabilization by the glmS ribozyme. Genes Dev 21:3356–3368
Coppins RL, Hall KB, Groisman EA (2007) The intricate world of riboswitches. Curr Opin Microbiol 10:176–181
Curtis EA, Bartel DP (2001) The hammerhead cleavage reaction in monovalent cations. RNA 7:546–552
Das S, Piccirilli J (2005) General acid catalysis by the hepatitis delta virus ribozyme. Nat Chem Biol 1:45–52
De la Pena M, Gago S, Flores R (2003) Peripheral regions of natural hammerhead ribozymes greatly increase their self-cleavage activity. EMBO J 22:5561–5570
Ditzler MA, Aleman EA, Rueda D, Walter NG (2007) Focus on function: single molecule RNA enzymology. Biopolymers 87:302–316
Doudna JA, Lorsch JR (2005) Ribozyme catalysis: not different, just worse. Nat Struct Mol Biol 12:395–402
Draper DE, Grilley D, Soto AM (2005) Ions and RNA folding. Annu Rev Biophys Biomol Struct 34:221–243
Edwards TE, Klein DJ, Ferre-D'Amare AR (2007) Riboswitches: small-molecule recognition by gene regulatory RNAs. Curr Opin Struct Biol 17:273–279
Emilsson GM, Nakamura S, Roth A, Breaker RR (2003) Ribozyme speed limits. RNA 9: 907–918
Fedor MJ, Williamson JR (2005) The catalytic diversity of RNAs. Nat Rev Mol Cell Biol 6: 399–412
Feldstein PA, Buzayan JM, van Tol H, deBear J, Gough GR, Gilham PT, Bruening G (1990) Specific association between an endoribonucleolytic sequence from a satellite RNA and a substrate analogue containing a 2′-5′ phosphodiester. Proc Natl Acad Sci U S A 87: 2623–2627
Ferre-D'Amare AR, Doudna JA (2000) Crystallization and structure determination of a hepatitis delta virus ribozyme: use of the RNA-binding protein U1A as a crystallization module. J Mol Biol 295:541–556
Ferre-D'Amare AR, Zhou K, Doudna JA (1998) Crystal structure of a hepatitis delta virus ribozyme. Nature 395:567–574
Flores R, Delgado S, Gas ME, Carbonell A, Molina D, Gago S, De la Pena M (2004) Viroids: the minimal non-coding RNAs with autonomous replication. FEBS Lett 567:42–48
Förster T (1946) Energiewanderung Und Fluoreszenz. Naturwissenschaften 33:166–175
Förster T (1948) Intermolecular energy migration and fluorescence. Ann Phys (Leipzig) 2:55–75
Forster AC, Symons RH (1987) Self-cleavage of virusoid RNA is performed by the proposed 55-nucleotide active site. Cell 50:9–16
Furtig B, Richter C, Schell P, Wenter P, Pitsch S, Schwalbe H (2008) NMR-spectroscopic characterisation of phosphodiester bond cleavage catalysed by the minimal hammerhead ribozyme. RNA Biol 5:41–48
Gong B, Chen JH, Chase E, Chadalavada DM, Yajima R, Golden BL, Bevilacqua PC, Carey PR (2007) Direct measurement of a pK(a) near neutrality for the catalytic cytosine in the genomic HDV ribozyme using Raman crystallography. J Am Chem Soc 129:13335–13342
Guerrier-Takada C, Gardiner K, Marsh T, Pace N, Altman S (1983) The RNA moiety of ribonuclease P is the catalytic subunit of the enzyme. Cell 35:849–857
Hammann C, Lilley DM (2002) Folding and activity of the hammerhead ribozyme. Chembiochem 3:690–700
Hammes-Schiffer S, Benkovic SJ (2006) Relating protein motion to catalysis. Annu Rev Biochem 75:519–541

Hampel A, Cowan JA (1997) A unique mechanism for RNA catalysis: the role of metal cofactors in hairpin ribozyme cleavage. Chem Biol 4:513–517
Hampel KJ, Tinsley MM (2006) Evidence for preorganization of the glmS ribozyme ligand binding pocket. Biochemistry 45:7861–7871
Haran G (2004) Noise reduction in single-molecule fluorescence trajectories of folding proteins. Chem Phys 307:137–145
Harris DA, Rueda D, Walter NG (2002) Local conformational changes in the catalytic core of the trans-acting hepatitis delta virus ribozyme accompany catalysis. Biochemistry 41: 12051–12061
Haseloff J, Gerlach WL (1989) Sequences required for self-catalysed cleavage of the satellite RNA of tobacco ringspot virus. Gene 82:43–52
Hiley SL, Collins RA (2001) Rapid formation of a solvent-inaccessible core in the Neurospora Varkud satellite ribozyme. EMBO J 20:5461–5469
Hiley SL, Sood VD, Fan J, Collins RA (2002) 4-thio-U cross-linking identifies the active site of the VS ribozyme. EMBO J 21:4691–4698
Jaikaran D, Smith MD, Mehdizadeh R, Olive J, Collins RA (2008) An important role of G638 in the cis-cleavage reaction of the Neurospora VS ribozyme revealed by a novel nucleotide analog incorporation method. RNA 14:938–949
Jeong S, Sefcikova J, Tinsley RA, Rueda D, Walter NG (2003) Trans-acting hepatitis delta virus ribozyme: catalytic core and global structure are dependent on the 5′ substrate sequence. Biochemistry 42:7727–7740
Kaukinen U, Lyytikainen S, Mikkola S, Lonnberg H (2002) The reactivity of phosphodiester bonds within linear single-stranded oligoribonucleotides is strongly dependent on the base sequence. Nucleic Acids Res 30:468–474
Ke A, Zhou K, Ding F, Cate JH, Doudna JA (2004) A conformational switch controls hepatitis delta virus ribozyme catalysis. Nature 429:201–205
Khvorova A, Lescoute A, Westhof E, Jayasena SD (2003) Sequence elements outside the hammerhead ribozyme catalytic core enable intracellular activity. Nat Struct Biol 10:708–712
Klein DJ, Ferre-D'Amare AR (2006) Structural basis of glmS ribozyme activation by glucosamine-6-phosphate. Science 313:1752–1756
Kruger K, Grabowski PJ, Zaug AJ, Sands J, Gottschling DE, Cech TR (1982) Self-splicing RNA: autoexcision and autocyclization of the ribosomal RNA intervening sequence of Tetrahymena. Cell 31:147–157
Kuzmin YI, Da Costa CP, Fedor MJ (2004) Role of an active site guanine in hairpin ribozyme catalysis probed by exogenous nucleobase rescue. J Mol Biol 340:233–251
Kuzmin YI, Da Costa CP, Cottrell JW, Fedor MJ (2005) Role of an active site adenine in hairpin ribozyme catalysis. J Mol Biol 349:989–1010
Lafontaine DA, Norman DG, Lilley DM (2001) Structure, folding and activity of the VS ribozyme: importance of the 2- 3–6 helical junction. EMBO J 20:1415–1424
Lafontaine DA, Norman DG, Lilley DM (2002) The global structure of the VS ribozyme. EMBO J 21:2461–2471
Lakowicz JR (2006) Principles of fluorescence spectroscopy, 3rd edn. Springer, New York
Liu S, Bokinsky G, Walter NG, Zhuang X (2007) Dissecting the multistep reaction pathway of an RNA enzyme by single-molecule kinetic "fingerprinting". Proc Natl Acad Sci U S A 104:12634–12639
Luptak A, Ferre-D'Amare AR, Zhou K, Zilm KW, Doudna JA (2001) Direct pK(a) measurement of the active-site cytosine in a genomic hepatitis delta virus ribozyme. J Am Chem Soc 123:8447–8452
Martick M, Scott WG (2006) Tertiary contacts distant from the active site prime a ribozyme for catalysis. Cell 126:309–320
Martick M, Lee TS, York DM, Scott WG (2008a) Solvent structure and hammerhead ribozyme catalysis. Chem Biol 15:332–342
Martick M, Horan LH, Noller HF, Scott WG (2008b) A discontinuous hammerhead ribozyme embedded in a mammalian messenger RNA. Nature 454:899–902

McCarthy TJ, Plog MA, Floy SA, Jansen JA, Soukup JK, Soukup GA (2005) Ligand requirements for glmS ribozyme self-cleavage. Chem Biol 12:1221–1226
McKay DB (1996) Structure and function of the hammerhead ribozyme: an unfinished story. RNA 2:395–403
Min D, Xue S, Li H, Yang W (2007) 'In-line attack' conformational effect plays a modest role in an enzyme-catalyzed RNA cleavage: a free energy simulation study. Nucleic Acids Res 35:4001–4006
Murchie AI, Thomson JB, Walter F, Lilley DM (1998) Folding of the hairpin ribozyme in its natural conformation achieves close physical proximity of the loops. Mol Cell 1:873–881
Murray JB, Seyhan AA, Walter NG, Burke JM, Scott WG (1998) The hammerhead, hairpin and VS ribozymes are catalytically proficient in monovalent cations alone. Chem Biol 5:587–595
Nahas MK, Wilson TJ, Hohng S, Jarvie K, Lilley DM, Ha T (2004) Observation of internal cleavage and ligation reactions of a ribozyme. Nat Struct Mol Biol 11:1107–1113
Nakano S, Bevilacqua PC (2007) Mechanistic characterization of the HDV genomic ribozyme: a mutant of the C41 motif provides insight into the positioning and thermodynamic linkage of metal ions and protons. Biochemistry 46:3001–3012
Nakano S, Chadalavada DM, Bevilacqua PC (2000) General acid-base catalysis in the mechanism of a hepatitis delta virus ribozyme. Science 287:1493–1497
Nakano S, Cerrone AL, Bevilacqua PC (2003) Mechanistic characterization of the HDV genomic ribozyme: classifying the catalytic and structural metal ion sites within a multichannel reaction mechanism. Biochemistry 42:2982–2994
Nelson JA, Uhlenbeck OC (2006) When to believe what you see. Mol Cell 23:447–450
Nelson JA, Uhlenbeck OC (2008a) Hammerhead redux: does the new structure fit the old biochemical data? RNA 14:605–615
Nelson JA, Uhlenbeck OC (2008b) Minimal and extended hammerheads utilize a similar dynamic reaction mechanism for catalysis. RNA 14:43–54
Nesbitt S, Hegg LA, Fedor MJ (1997) An unusual pH-independent and metal-ion-independent mechanism for hairpin ribozyme catalysis. Chem Biol 4:619–630
O'Rear JL, Wang S, Feig AL, Beigelman L, Uhlenbeck OC, Herschlag D (2001) Comparison of the hammerhead cleavage reactions stimulated by monovalent and divalent cations. RNA 7(4):537–545
Okumus B, Wilson TJ, Lilley DM, Ha T (2004) Vesicle encapsulation studies reveal that single molecule ribozyme heterogeneities are intrinsic. Biophys J 87:2798–2806
Penedo JC, Wilson TJ, Jayasena SD, Khvorova A, Lilley DM (2004) Folding of the natural hammerhead ribozyme is enhanced by interaction of auxiliary elements. RNA 10:880–888
Pereira MJ, Harris DA, Rueda D, Walter NG (2002) Reaction pathway of the trans-acting hepatitis delta virus ribozyme: a conformational change accompanies catalysis. Biochemistry 41: 730–740
Pereira MJB, Nikolova EN, Hiley SL, Collins RA, Walter NG (2008) Single VS ribozyme molecules reveal dynamic and hierarchical folding toward catalysis. J Mol Biol 382:496–509
Perrotta AT, Been MD (1991) A pseudoknot-like structure required for efficient self-cleavage of hepatitis delta virus RNA. Nature 350:434–436
Perrotta AT, Shih I, Been MD (1999) Imidazole rescue of a cytosine mutation in a self-cleaving ribozyme. Science 286:123–126
Pinard R, Hampel KJ, Heckman JE, Lambert D, Chan PA, Major F, Burke JM (2001) Functional involvement of G8 in the hairpin ribozyme cleavage mechanism. EMBO J 20:6434–6442
Prody GA, Bakos JT, Buzayan JM, Schneider IR, Bruening G (1986) Autolytic Processing of Dimeric Plant Virus Satellite RNA. Science 231:1577–1580
Pyle AM (1993) Ribozymes: a distinct class of metalloenzymes. Science 261:709–714
Rastogi T, Beattie TL, Olive JE, Collins RA (1996) A long-range pseudoknot is required for activity of the Neurospora VS ribozyme. EMBO J 15:2820–2825
Rhodes MM, Reblova K, Sponer J, Walter NG (2006) Trapped water molecules are essential to structural dynamics and function of a ribozyme. Proc Natl Acad Sci U S A 103:13380–13385

Roth A, Nahvi A, Lee M, Jona I, Breaker RR (2006) Characteristics of the glmS ribozyme suggest only structural roles for divalent metal ions. RNA 12:607–619

Rueda D, Wick K, McDowell SE, Walter NG (2003) Diffusely bound $Mg2^{+}$ ions slightly reorient stems I and II of the hammerhead ribozyme to increase the probability of formation of the catalytic core. Biochemistry 42:9924–9936

Rueda D, Bokinsky G, Rhodes MM, Rust MJ, Zhuang X, Walter NG (2004) Single-molecule enzymology of RNA: essential functional groups impact catalysis from a distance. Proc Natl Acad Sci U S A 101:10066–10071

Ruffner DE, Stormo GD, Uhlenbeck OC (1990) Sequence requirements of the hammerhead RNA self-cleavage reaction. Biochemistry 29:10695–10702

Rupert PB, Ferre-D'Amare AR (2001) Crystal structure of a hairpin ribozyme-inhibitor complex with implications for catalysis. Nature 410:780–786

Rupert PB, Massey AP, Sigurdsson ST, Ferre-D'Amare AR (2002) Transition state stabilization by a catalytic RNA. Science 298:1421–1424

Salehi-Ashtiani K, Szostak JW (2001) In vitro evolution suggests multiple origins for the hammerhead ribozyme. Nature 414:82–84

Salehi-Ashtiani K, Luptak A, Litovchick A, Szostak JW (2006) A genomewide search for ribozymes reveals an HDV-like sequence in the human CPEB3 gene. Science 313:1788–1792

Salter J, Krucinska J, Alam S, Grum-Tokars V, Wedekind JE (2006) Water in the active site of an all-RNA hairpin ribozyme and effects of Gua8 base variants on the geometry of phosphoryl transfer. Biochemistry 45:686–700

Saville BJ, Collins RA (1990) A site-specific self-cleavage reaction performed by a novel RNA in Neurospora mitochondria. Cell 61:685–696

Scott WG (2007) Ribozymes. Curr Opin Struct Biol 17:280–286

Sefcikova J, Krasovska MV, Sponer J, Walter NG (2007) The genomic HDV ribozyme utilizes a previously unnoticed U-turn motif to accomplish fast site-specific catalysis. Nucleic Acids Res 35:1933–1946

Simorre JP, Legault P, Hangar AB, Michiels P, Pardi A (1997) A conformational change in the catalytic core of the hammerhead ribozyme upon cleavage of an RNA substrate. Biochemistry 36:518–525

Simorre JP, Legault P, Baidya N, Uhlenbeck OC, Maloney L, Wincott F, Usman N, Beigelman L, Pardi A (1998) Structural variation induced by different nucleotides at the cleavage site of the hammerhead ribozyme. Biochemistry 37:4034–4044

Smith MD, Collins RA (2007) Evidence for proton transfer in the rate-limiting step of a fast-cleaving Varkud satellite ribozyme. Proc Natl Acad Sci U S A 104:5818–5823

Stryer L (1978) Fluorescence energy transfer as a spectroscopic ruler. Annu Rev Biochem 47:819–846

Taylor JM (2006) Structure and replication of hepatitis delta virus RNA. Curr Top Microbiol Immunol 307:1–23

Tinsley RA, Walter NG (2007) Long-range impact of peripheral joining elements on structure and function of the hepatitis delta virus ribozyme. Biol Chem 388:705–715

Tinsley RA, Harris DA, Walter NG (2004) Magnesium dependence of the amplified conformational switch in the trans-acting hepatitis delta virus ribozyme. Biochemistry 43:8935–8945

Tinsley RA, Furchak JR, Walter NG (2007) Trans-acting glmS catalytic riboswitch: locked and loaded. Rna 13:468–477

Torelli AT, Krucinska J, Wedekind JE (2007) A comparison of vanadate to a 2′-5′ linkage at the active site of a small ribozyme suggests a role for water in transition-state stabilization. RNA 13:1052–1070

Tuschl T, Gohlke C, Jovin TM, Westhof E, Eckstein F (1994) A three-dimensional model for the hammerhead ribozyme based on fluorescence measurements. Science 266:785–789

Walter NG (2001) Structural dynamics of catalytic RNA highlighted by fluorescence resonance energy transfer. Methods 25:19–30

Walter NG (2002) Probing RNA structural dynamics and function by fluorescence resonance energy transfer (FRET). Curr Protoc Nucleic Acid Chem 11.10:11.0.1–0.23

Walter NG (2007) Ribozyme catalysis revisited: is water involved? Mol Cell 28:923–929
Walter NG, Burke JM (1998) The hairpin ribozyme: structure, assembly and catalysis. Curr Opin Chem Biol 2:24–30
Walter F, Murchie AI, Thomson JB, Lilley DM (1998a) Structure and activity of the hairpin ribozyme in its natural junction conformation: effect of metal ions. Biochemistry 37:14195–14203
Walter F, Murchie AIH, Lilley DMJ (1998b) Folding of the four-way RNA junction of the hairpin ribozyme. Biochemistry 37:17629–17636
Walter NG, Hampel KJ, Brown KM, Burke JM (1998c) Tertiary structure formation in the hairpin ribozyme monitored by fluorescence resonance energy transfer. EMBO J 17:2378–2391
Walter NG, Burke JM, Millar DP (1999) Stability of hairpin ribozyme tertiary structure is governed by the interdomain junction. Nat Struct Biol 6:544–549
Walter NG, Huang C, Manzo AJ, Sobhy MA (2008) Do-it-yourself guide: how to use the modern single molecule toolkit. Nat Methods 5:475–489
Wedekind JE, McKay DB (1998) Crystallographic structures of the hammerhead ribozyme: relationship to ribozyme folding and catalysis. Annu Rev Biophys Biomol Struct 27:475–502
Wilson TJ, Ouellet J, Zhao ZY, Harusawa S, Araki L, Kurihara T, Lilley DM (2006) Nucleobase catalysis in the hairpin ribozyme. RNA 12:980–987
Wilson TJ, McLeod AC, Lilley DM (2007) A guanine nucleobase important for catalysis by the VS ribozyme. Embo J 26:2489–2500
Winkler WC, Breaker RR (2005) Regulation of bacterial gene expression by riboswitches. Annu Rev Microbiol 59:487–517
Winkler WC, Nahvi A, Roth A, Collins JA, Breaker RR (2004) Control of gene expression by a natural metabolite-responsive ribozyme. Nature 428:281–286
Young KJ, Gill F, Grasby JA (1997) Metal ions play a passive role in the hairpin ribozyme catalysed reaction. Nucleic Acids Res 25:3760–3766
Zhou DM, Taira K (1998) The hydrolysis of RNA: from theoretical calculations to the hammerhead ribozyme-mediated cleavage of RNA. Chem Rev 98:991–1026
Zhuang X (2005) Single-molecule RNA science. Annu Rev Biophys Biomol Struct 34:399–414
Zhuang X, Kim H, Pereira MJ, Babcock HP, Walter NG, Chu S (2002) Correlating structural dynamics and function in single ribozyme molecules. Science 296:1473–1476